Notch signaling is necessary for epithelial growth arrest by TGF-β

Hideki Niimi, Katerina Pardali, Michael Vanlandewijck, Carl-Henrik Heldin, and Aristidis Moustakas

Ludwig Institute for Cancer Research, Biomedical Center, Uppsala University, SE-751 24 Uppsala, Sweden

Transforming growth factor β (TGF-β) and Notch act as tumor suppressors by inhibiting epithelial cell proliferation. TGF-β additionally promotes tumor invasiveness and metastasis, whereas Notch supports oncogenic growth. We demonstrate that TGF-β and ectopic Notch1 receptor cooperatively arrest epithelial growth, whereas endogenous Notch signaling was found to be required for TGF-β to elicit cytostasis. Transcriptomic analysis after blocking endogenous Notch signaling uncovered several genes, including Notch pathway components and cell cycle and apoptosis factors, whose regulation by TGF-β requires an active Notch pathway. A prominent gene coregulated by the two pathways is the cell cycle inhibitor *p21*. Both transcriptional induction of the Notch ligand Jagged1 by TGF-β and endogenous levels of the Notch effector CSL contribute to p21 induction and epithelial cytostasis. Cooperative inhibition of cell proliferation by TGF-β and Notch is lost in human mammary cells in which the *p21* gene has been knocked out. We establish an intimate involvement of Notch signaling in the epithelial cytostatic response to TGF-β.

Introduction

TGF-β inhibits cell growth and acts as a tumor suppressor (Levy and Hill, 2006). TGF-β signals via receptor serine/threonine kinases that phosphorylate Smad proteins, which move to the nucleus and regulate gene transcription (Massagué et al., 2005). During epithelial cytostasis (growth arrest), Smads induce cell cycle inhibitors *p15* and *p21* and repress *c-Myc* and inhibitors of differentiation *Id1*, *Id2*, and *Id3* (Pardali and Moustakas, 2007). TGF-β up-regulates rapidly and maintains prolonged *p21* mRNA and protein levels, which is critical for epithelial cytostasis (Nicolas and Hill, 2003; Pardali et al., 2005). The mechanism of sustained p21 maintenance is not clear, and we hypothesized that it could be achieved by a secondary wave of TGF-β signaling that activates new factors capable of maintaining p21 levels. A candidate pathway for involvement in such a scenario is Notch, a major regulator of cell fate (Lai, 2004).

Four distinct mammalian receptors (Notch1–4) interact extracellularly with transmembrane ligands Jagged1, 2, and Deltalike1–3 (DLL1–3), which are expressed by adjacent cells (Lai, 2004). Such an interaction leads to the proteolytic cleavage of Notch by the γ-secretase activity of presenilin, thus releasing the Notch intracellular domain, which enters the nucleus and regulates transcription after binding to the transcription factor CSL (Lai, 2004).

Retroviral insertions in mice and chromosomal translocations in human leukemias cause oncogenic truncations or fusions of Notch (Radtke and Raj, 2003). The skin- or liver-specific knockout of Notch1 leads to tumorigenesis, classifying Notch1 as a tumor suppressor (Nicolas et al., 2003; Croquelois et al., 2005). Notch1 inhibits epidermal, endothelial, and hepatic cell growth (Rangarajan et al., 2001; Qi et al., 2003; Noseda et al., 2004). Notch arrests the keratinocyte cell cycle by transcriptionally inducing *p21* via CSL or calcineurin–nuclear factor of activated T cells pathway activation (Rangarajan et al., 2001; Mammucari et al., 2005).

Notch and TGF-β pathways cross talk, as TGF-β induces Jagged1 expression, leading to epithelial-mesenchymal transition (Zavadil et al., 2004). During heart organogenesis, Notch uses TGF-β signaling to cause the epithelial-mesenchymal transition (Timmerman et al., 2004). Alternatively, Notch induces nodal, a TGF-β family regulator of embryogenesis (Raya et al., 2003). The Notch intracellular domain directly binds to Smads, leading to the coregulation of gene expression in neuronal and endothelial cells (Blokzijl et al., 2003; Itoh et al., 2004).

Based on these facts, we investigated cross talk between TGF-β and Notch during epithelial cytostasis. We demonstrate that the TGF-β cytostatic response at least partly requires Notch signaling. A novel mechanism based on transcriptional induction of the Notch ligand Jagged1, involvement of the Notch effector CSL, and sustained p21 induction explains the interdependent roles of TGF-β and Notch during cytostasis.

Results

Notch and TGF-β cooperatively arrest epithelial cell growth

To study cross talk between Notch and TGF-β, we ectopically expressed the human Notch1 intracellular domain (N1ICD; Rangarajan et al., 2001). Usually, 70–80% of cells expressed N1ICD at roughly endogenous levels, which induced a classic target of this pathway (transcription factor *Hes1*; unpublished data). In mock-infected (Ad-GFP) mouse mammary epithelial

NMuMG cells, TGF-β1 suppressed S-phase entry by 60–70% (Fig. 1 A). Ectopic N1ICD did not have much effect on its own, but N1ICD plus TGF-β1 suppressed S-phase entry by 80–95% (Fig. 1 A). This effect was dependent on TGF-β1 dose (Fig. S1 A, available at http://www.jcb.org/cgi/content/full/jcb.200612129/DC1) and was also confirmed in human mammary MCF-10A cells (see Fig. 8 A).

TGF-β1 stimulation in the presence of a γ-secretase inhibitor (GSI), which blocks endogenous Notch signaling (Brunkan and Goate, 2005), led to a substantial but not complete restoration of S-phase entry (Fig. 1 B), which was confirmed in the mammary epithelial MCF-10A cells (see Fig. 8 C) and in immortalized human mammary epithelial cells (HMECs; Fig. S1 B). In contrast, in mink lung epithelial cells, ectopic N1ICD inhibited the suppressive effect of TGF-β1 (Fig. S1 C). This highlights the cell context dependency of the cytostatic response and confirms a recent study that shows c-Myc up-regulation by Notch signaling, which counteracts cytostasis by TGF-β (Rao and Kadesch, 2003).

In human HaCaT keratinocytes, Ad-N1ICD alone suppressed S-phase entry almost to the same extent as 2 ng/ml TGF-β1 (Fig. 1 C). Ad-N1ICD combined with TGF-β1 led to >95% growth suppression, and up to 80% of the cells were arrested in G1 phase of the cell cycle (Fig. 1 E). This showed strong Notch1–TGF-β1 cooperativity that was blocked by TGF-β receptor kinase inhibitors (Fig. S1 D), suggesting the interdependence of the two pathways. GSI also blocked cytostasis by TGF-β1 in HaCaT cells (Figs. 1 D and S1 E) and shifted the cell cycle profile to that of mock-treated cells (Fig. 1 F). We conclude that Notch and TGF-β cooperatively induce growth arrest in human and mouse epithelial cells of mammary and skin origin. Endogenous Notch signaling is partly necessary for growth arrest by TGF-β.

Notch signaling is required for the regulation of many genes by TGF-β

To further understand the Notch–TGF-β cross talk, we performed a transcriptomic screen in HaCaT cells stimulated with TGF-β1 in the absence or presence of GSI. We measured gene expression after cycloheximide pretreatment after 2, 6, and 48 h of TGF-β1 stimulation, aiming at immediate/early, intermediate, and sustained gene responses. Several hundred TGF-β–responsive genes were measured (Fig. 2 A and Table S1, available at http://www.jcb.org/cgi/content/full/jcb.200612129/DC1), which is in accordance with previous microarray analyses in the same cell line (Akiyoshi et al., 2001; Zavadil et al., 2001; Kang et al., 2003). GSI decreased the number of TGF-β–regulated genes by 36% (Fig. 2 A and Table S1). At 2 h, only immediate/early TGF-β gene targets were measured, and GSI had no effect. At 6 h, we observed 85% inhibition. At 48 h, we did not observe dramatic effects on total gene numbers, but effects were seen on individual gene profiles.

A comparison of the two gene lists (minus and plus GSI) showed 198 genes whose response to TGF-β was unaffected by GSI (Fig. 2, B and C). Examples are *TIEG* (TGF-β–inducible early growth response protein 1), a zinc finger transcription and proapoptotic factor; *TNFSF10* (TNF ligand superfamily member 10),
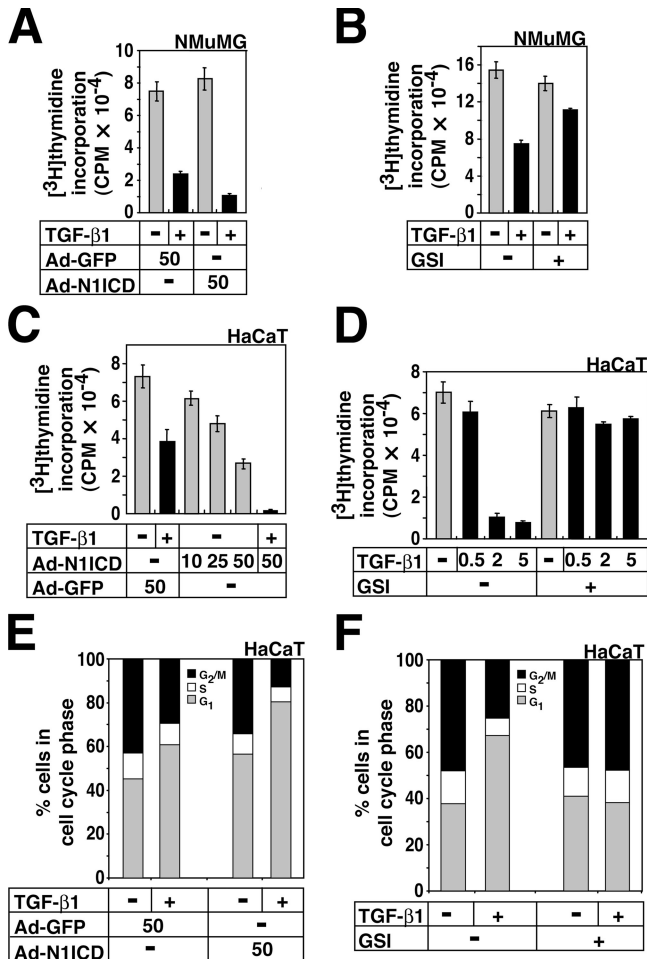
Figure 1. **Notch and TGF-β cooperate during epithelial growth arrest.** (A–D) Thymidine incorporation assays in NMuMG (A and B) or HaCaT (C and D) cells infected with Ad-GFP or Ad-N1ICD (multiplicity of infection [MOI] of 50) and stimulated with vehicle (−) or 2 ng/ml TGF-β1 for 60 h (A and C) or stimulated with TGF-β1 in the presence or absence of 4 μM GSI (B and D). In D, 0.5–5 ng/ml TGF-β1 was used. (E and F) HaCaT cell cycle analysis under conditions as in C and D. The percentage of cells per cell cycle phase is plotted in bar graphs. Error bars represent SD.

a proapoptotic secreted protein; *NF2* (neurofibromin 2), a cytoskeletal regulator; and *IFITM* (interferon-induced transmembrane protein 1), a cell surface antigen. The expression of 394 TGF-β1–responsive genes (roughly 50% of the regulated genes) was neutralized by GSI, demonstrating a strong dependency on Notch (Fig. 2, B and C). Examples are *STRAP* (serine-threonine kinase receptor-associated protein), an adaptor that binds to TGF-β receptor and inhibitory Smad7 to mediate the termination of TGF-β signaling; *SMURF1* (Smad ubiquitylation regulatory factor 1), an E3 ubiquitin ligase that causes TGF-β receptor and Smad degradation; *S100A11*, a calcium-binding protein that mediates epithelial cytostasis by TGF-β as it transcriptionally induces the cell cycle inhibitor *p21*; and *IVL* (involucrin), a keratinocyte differentiation marker that cross-links to the keratin cytoskeleton. Finally, 179 genes were not previously recognized as TGF-β targets, as their regulation is revealed only after GSI treatment (Fig. 2 B), suggesting that Notch signaling may repress genes in a manner that prohibits responses to TGF-β. This experimental design did not test for adverse effects of GSI on gene expression in general, which is formally possible. However, GSI both inhibited and induced specific gene expression when combined with TGF-β, and we never observed adverse effects of GSI in the absence of TGF-β in RT-PCR assays.

For the first time, we uncovered large gene sets that are co-regulated by TGF-β and Notch positively or negatively (Fig. 2 and Table S1). Notch seemed to counteract the regulation of many genes by TGF-β1. This suggests that to a large extent, the transcriptomic response to TGF-β incorporates regulation by Notch signaling.

TGF-β1 induces the expression of Notch ligands and modulates the Notch receptor profile

Among the genes identified, two were members of the Notch pathway: TGF-β1 induced *JAGGED1* (*JAG1*) and repressed *NOTCH1* (Fig. 3 A). We examined whether TGF-β1 regulates the expression of all Notch ligands and receptors in HaCaT (Fig. 3, B and C) and NMuMG cells (Fig. S2, available at http://www.jcb.org/cgi/content/full/jcb.200612129/DC1). TGF-β1 considerably induced *JAG1* mRNA and protein and *DLL4* mRNA, weakly induced *DLL3* mRNA at 24 h, and did not appreciably affect *JAG2* or *DLL1* mRNA in HaCaT cells. In NMuMG cells, TGF-β1 induced *Jag1* mRNA and protein and *Dll1* mRNA but did not appreciably regulate *Jag2* mRNA levels (Fig. S2, A and B). On the other hand, TGF-β1 repressed *NOTCH1* mRNA and protein in HaCaT cells (Fig. 3, B and C). Even more dramatic was *NOTCH3* repression by TGF-β1 in the same cells (Fig. 3, B and C). *NOTCH2* and *NOTCH4* expression was not appreciably affected by TGF-β1 in HaCaT cells (Fig. 3 B). Although similar HaCaT expression profiles were measured for the *Notch1* receptor in NMuMG cells responding to TGF-β1, *Notch4* mRNA and protein were considerably induced in NMuMG cells (Fig. S2, C and D).

In HaCaT cells, GSI primarily perturbed the expression profile of *JAG1* and, to a lesser extent, that of *NOTCH3* (Fig. 3, B and C), weakly induced *DLL1* at 24 h, and repressed

the weak induction of *DLL3* at 24 h but did not affect the other regulated ligands or receptors. This agrees with the effect of cycloheximide that blocks the induction of *JAG1*, *DLL1*, and *DLL3* by TGF-β1 (unpublished data), which represents indirect Notch-mediated responses to TGF-β. The lack of effect of GSI on Notch receptor profiles is also seen at the protein levels of TβRI, which is slowly down-regulated during the time course but is not affected by GSI (Fig. 3 C). We conclude that TGF-β1 induces the expression of endogenous Notch ligands in keratinocytes and mammary epithelial cells, whereas the regulation of Notch receptors is complex and tissue type dependent. Between the two regulated ligands JAG1 and DLL4, we could only verify the regulation of JAG1 protein (Fig. 3 C), as our DLL4 antibody showed poor efficacy (unpublished data). Thus, during the stimulation of epithelial cells with TGF-β, the initial induction of various Notch ligands may activate this pathway, whereas the delayed repression of Notch receptors may reflect a negative loop of Notch receptor down-regulation.
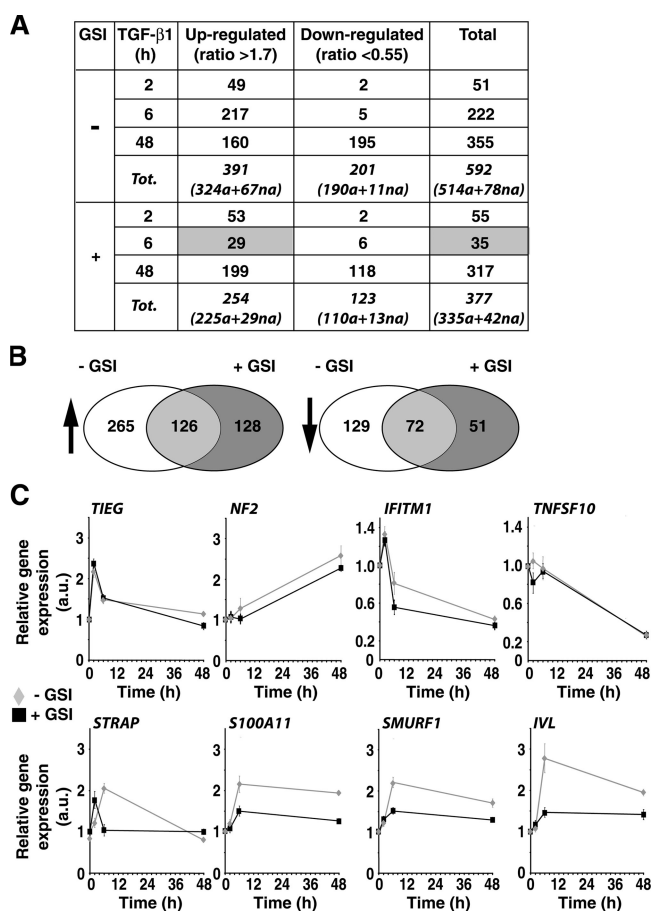
A

GSI	TGF-β1 (h)	Up-regulated (ratio >1.7)	Down-regulated (ratio <0.55)	Total
	2	49	2	51
−	6	217	5	222
	48	160	195	355
	Tot.	*391 (324a+67na)*	*201 (190a+11na)*	*592 (514a+78na)*
	2	53	2	55
+	6	29	6	35
	48	199	118	317
	Tot.	*254 (225a+29na)*	*123 (110a+13na)*	*377 (335a+42na)*

B

C

Figure 2. **Transcriptomic analysis of the dependence of TGF-β1 on Notch signaling.** (A and B) Cumulative gene expression data from HaCaT cells (A) and Venn diagrams (B) that cluster genes to each category of cell treatment. The total (Tot) gene numbers indicate the number of annotated (a) and nonannotated (na) genes. Gray table cells indicate significant deviations (P < 0.01) upon GSI treatment relative to the control. In B, up- and down-regulated (arrows) gene numbers are shown within each Venn diagram. (C) Kinetic graphs of eight representative genes with expression values (arbitrary units [au]) calculated from the microarray data. Error bars represent SD.
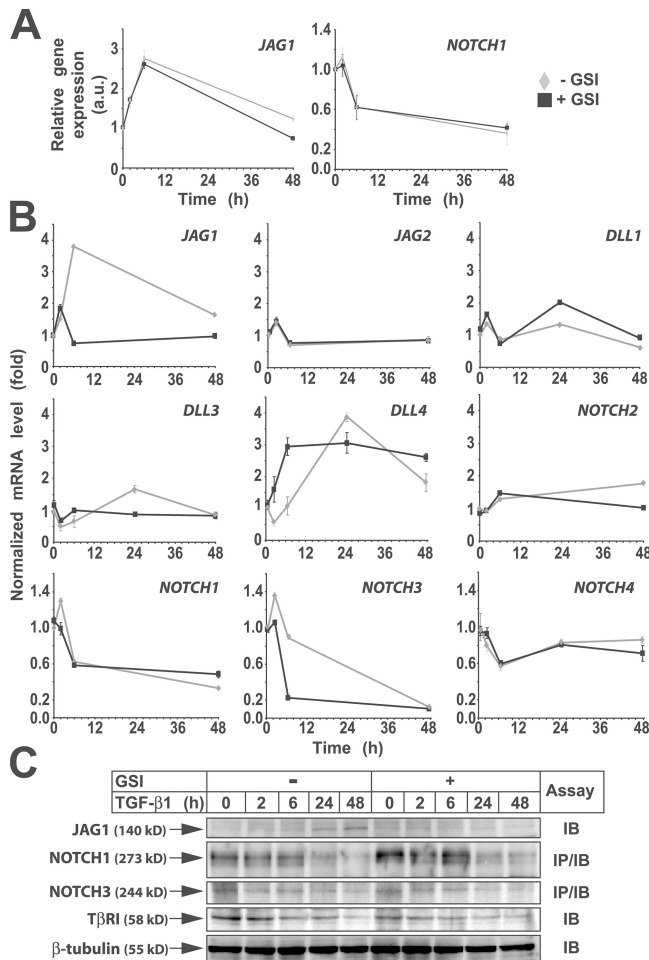
Figure 3. **TGF-β1 regulates the expression of Notch ligands and receptors.** (A) Kinetic expression profiles of *JAG1* and *NOTCH1* measured via microarray analysis (expressed in arbitrary units [au]). (B) Quantitative RT-PCR of *JAG1,2*, *DLL1,2,3*, and *NOTCH1,2,3,4* mRNAs in HaCaT cells stimulated with 2 ng/ml TGF-β1 for 2, 6, 24, and 48 h in the absence (DMSO, −; gray lines) or presence of 4 μM GSI (+; black lines). Relative gene expression values (fold change) after normalization to *GAPDH* gene expression are shown. (C) Immunoblot analysis of JAG1, NOTCH1, NOTCH3, TβRI, and control β-tubulin protein levels from HaCaT cells treated with TGF-β1 and GSI as indicated. Immunoblots of total cell lysates (IB) or immunoblots after immunoprecipitation (IP/IB) are shown. Error bars represent SD.

TGF-β target genes that regulate the cell cycle or induce apoptosis

11 genes with known links to the cytostatic and apoptotic programs of TGF-β were identified in the transcriptomic screen: the cell cycle inhibitors p21 (*CDKN1A*) and p15 (*CDKN2B*), cyclins B2 (*CCNB2*), D1 (*CCND1*), and D2 (*CCND2*), the transcriptional regulators c-Myc (*MYC*) and Id2 (*IDB2*), the signal transducer S100A11 (*S100A11*), and the apoptotic/survival regulators GADD45β (*GADD45B*), GADD45γ (*GADD45G*), and TIEG (*TIEG-1/KLF10*; Fig. 4 A). Prolonged up- or down-regulation of many of these genes was neutralized by GSI (Fig. 4 A) as verified by quantitative RT-PCR analysis (Fig. 4 B).

The *c-MYC* gene, a well studied transcriptional target of TGF-β/Smad signaling that plays major regulatory roles in the epithelial cytostatic program of TGF-β (Chen et al., 2002),

exhibited its characteristic repression phase followed by the recovery of basal mRNA levels after 24 h of TGF-β stimulation (Fig. 4 B). GSI did not affect the *c-MYC* expression profile, suggesting that endogenous Notch signaling is not involved in the *c-MYC* response of keratinocytes, which is in contrast to what was previously reported for mink lung epithelial cells that overexpressed N1ICD (Rao and Kadesch, 2003). Similar to *c-MYC*, cyclin B2 (*CCNB2*) also exhibited relative insensitivity to GSI throughout the time course. Among the 11 genes of the cytostatic/apoptotic program, GSI most prominently affected *p21*, *p15*, *IDB2*, *S100A11*, and *GADD45B* expression profiles from 6 h onwards (Fig. 4, A and B; *p21*, *p15*, and *GADD45B*). The immediate/early response of all the genes measured after 2 h of stimulation with TGF-β1 in the presence of cycloheximide was not substantially affected by GSI (Fig. 4, A and B).

GSI quantitatively reduced the amplitude of the mRNA profiles of the aforementioned genes (Fig. 4 B, *GADD45B* and *CDKN2B*) but preserved the dynamic changes in the overall profile of mRNA expression. In the case of the p21 cell cycle inhibitor, GSI not only reduced the amplitude of the response but also distorted the expression profile beyond 2 h dramatically (Fig. 4 B). Although the immediate/early response of *p21* to TGF-β1 was unaffected by GSI, long-term *p21* mRNA induction was substantially blocked by GSI, suggesting that Notch signaling was critical for this response, acting as a secondary signal to the primary TGF-β stimulus. The effect of GSI was also considerable at the protein level because sustained (6–24 h) p21 protein induction by TGF-β1 was converted to an early response (1.5–3 h) in the presence of GSI (Fig. 4 C). This prompted us to further analyze the profile of p21 expression and also test the functional relevance of this profile. The present data demonstrate that although endogenous Notch signaling contributes to regulation of a substantial subset of the TGF-β cytostatic gene program, Notch is not involved in the regulation of every gene in this program.

Induction of Jagged1 by TGF-β contributes to p21 gene regulation and epithelial cytostasis

The evidence so far has led to a working model in which TGF-β signaling induces Jagged1 production, which then leads to Notch receptor activation and further signaling via CSL, leading to regulation of the cell cycle inhibitors p15 and p21 and, thus, mediating epithelial cell cycle arrest (Fig. 5 A). To examine the functional relevance of *JAG1* induction by TGF-β during cytostasis, we depleted endogenous *JAG1* by siRNA (Fig. 5 B). The three- to fourfold induction of *JAG1* mRNA throughout the 24-h time course in response to TGF-β was reduced to a mere 1.3–1.6-fold induction in the presence of siRNA. Under the same conditions of endogenous *JAG1* depletion, JAG1 protein accumulation in the 6–24-h interval of the time course was severely lost to essentially undetectable levels (Fig. 5 C). The specificity of *JAG1* siRNA–mediated depletion was verified by demonstrating that three unrelated proteins, Smad2, Smad3, and α-tubulin, were not affected by the same siRNA. In addition to the total Smad2 and Smad3 levels, TGF-β–inducible phospho-Smad2 and -Smad3 levels were not appreciably affected by *JAG1* siRNA during the 24-h time course (Fig. 5 C). Notably, the
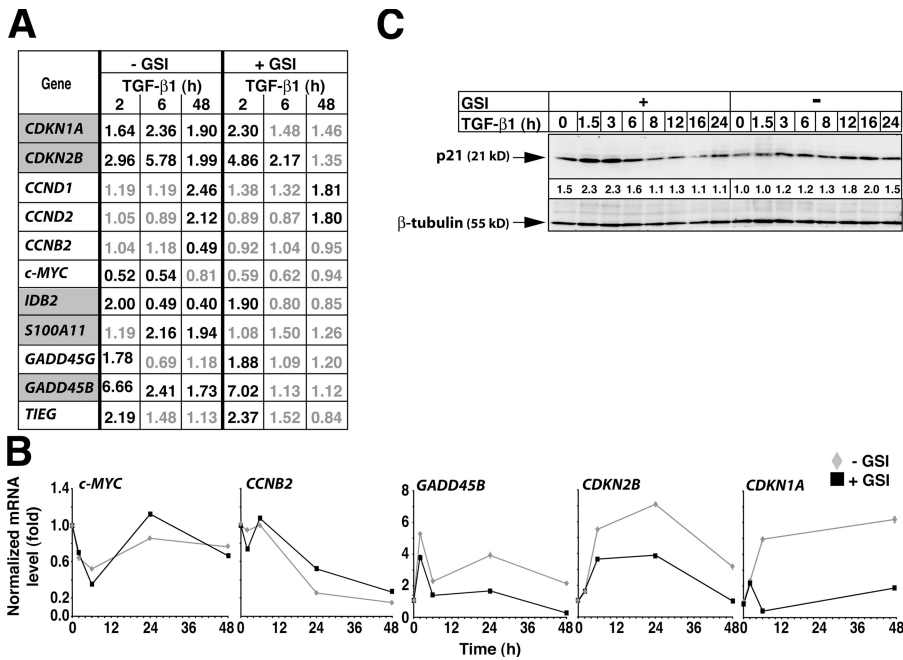
A

Gene	- GSI			+ GSI		
	TGF-β1 (h)			TGF-β1 (h)		
	2	6	48	2	6	48
CDKN1A	1.64	2.36	1.90	2.30	1.48	1.46
CDKN2B	2.96	5.78	1.99	4.86	2.17	1.35
CCND1	1.19	1.19	2.46	1.38	1.32	1.81
CCND2	1.05	0.89	2.12	0.89	0.87	1.80
CCNB2	1.04	1.18	0.49	0.92	1.04	0.95
c-MYC	0.52	0.54	0.81	0.59	0.62	0.94
IDB2	2.00	0.49	0.40	1.90	0.80	0.85
S100A11	1.19	2.16	1.94	1.08	1.50	1.26
GADD45G	1.78	0.69	1.18	1.88	1.09	1.20
GADD45B	6.66	2.41	1.73	7.02	1.13	1.12
TIEG	2.19	1.48	1.13	2.37	1.52	0.84

C

B

Figure 4. **TGF-β target genes of the cytostatic and apoptotic program and their dependence on Notch signaling.** (A) Table listing 11 regulated genes with links to cell cycle and apoptosis and statistically significant (black; $P < 0.05$) or nonsignificant (gray; $P > 0.05$) expression values. Gray cells indicate genes for which GSI treatment had a clear impact. (B) Quantitative RT-PCR of *c-Myc*, *CCNB2*, *GADD45B*, *CDKN2B*, and *CDKN1A* mRNAs in HaCaT cells treated as in Fig. 3 B. (C) Immunoblot of endogenous p21 and control β-tubulin in HaCaT cells stimulated with 2 ng/ml TGF-β1 for 0–24 h in the absence (−, DMSO) or presence (+) of 4 µM GSI.

knockdown of *JAG1* mRNA and protein resulted in a concomitant decrease in the TGF-β–inducible levels of *p21* mRNA and protein (Fig. 5, D and E). This decrease was evident throughout the time course and was more robust during the 6–24-h interval when endogenous JAG1 protein accumulated at maximal levels. Finally, we demonstrated that *JAG1* knockdown reverted the 70% growth inhibition by TGF-β1 to a mere 25% inhibition (Fig. 5 F), suggesting that endogenous JAG1 participates in the TGF-β cytostatic response. These data strongly suggest that transcriptional induction of the *JAG1* gene by TGF-β is intimately linked to the robust transcriptional induction of the p21 cell cycle inhibitor and to the growth inhibitory response of HaCaT keratinocytes (Fig. 5 A).

Importance of CSL during p21 induction and epithelial growth inhibition by TGF-β

Knockdown of endogenous Notch1 via siRNA was effective but failed to inactivate Notch signaling (unpublished data), as epithelial cells express other Notch receptors whose expression is regulated by TGF-β (Figs. 3 and S2). Therefore, we depleted CSL, which is the only known common mediator of all Notch signaling pathways. siRNA reduced *CSL* mRNA expression by 85% (Fig. 6 A) and reduced protein to undetectable levels (Fig. 6 F), whereas mock siRNA had no effect in HaCaT cells. The *CSL* knockdown was specific as verified by demonstrating that three unrelated proteins (Smad2, Smad3, and α-tubulin) were not affected by the same siRNA. In addition, the TGF-β–inducible phospho-Smad2 and -Smad3 levels were not appreciably affected by the *CSL* siRNA during the 48-h time course (Fig. 6 B). A comparable 65–75% knockdown of endogenous *CSL* was achieved when HaCaT cells were simultaneously infected with mock (Ad-GFP) or specific (Ad-N1ICD) adenoviruses (Fig. 6 C). During the concomitant stimulation of HaCaT cells with TGF-β1, we observed a minor trend for the induction of endogenous *CSL*

mRNA levels (Fig. 6, A and C), which we could not reproduce at the protein level (Fig. 6 F). As an additional confirmation of the specificity of *CSL* siRNA, ectopic *N1ICD* mRNA levels obtained after adenoviral infection of HaCaT cells were not affected by knocking down endogenous *CSL* (Fig. 6 D). Notably, under the same conditions of the combined knockdown of endogenous *CSL* and ectopic N1ICD expression, endogenous *p21* mRNA induction was dramatically reduced (Fig. 6 E). Under mock infection conditions, the 2.5–3-fold induction of endogenous *p21* mRNA by TGF-β1 was reduced to a weak 1.3-fold induction (Fig. 6 E), which was correspondingly reflected at the p21 protein level (Fig. 6 F). Furthermore, the synergistic *p21* induction by TGF-β1 and N1ICD also depended on proper endogenous *CSL* levels because knockdown of the latter considerably reduced the inducible *p21* mRNA levels (Fig. 6 E) and even more dramatically reduced the corresponding p21 protein levels (Fig. 6 F).

Finally, *CSL* knockdown substantially reverted cytostasis by TGF-β1; in mock-transfected cells, TGF-β1 stimulation caused a suppression of thymidine incorporation to 35% of unstimulated cells, whereas after CSL knockdown, the suppression was only to 64% of unstimulated cells (Fig. 6 G). In addition, *siCSL* reverted the cytostatic effect of N1ICD alone to control levels and strongly blocked synergistic cytostasis by TGF-β1 plus N1ICD (Fig. 6 G). These experiments with *CSL* knockdown demonstrate a similar phenotype to *JAG1* knockdown (Fig. 5) or the inhibition of γ-secretase activity by GSI (Figs. 1 and 4) and collectively prove that endogenous Notch/CSL signaling is critical, at least in part, for the antiproliferative response of HaCaT cells to TGF-β.

Partial dependence of TGF-β receptor signaling on γ-secretase activity

The γ-secretase activity of presenilin regulates Notch, Wnt/β-catenin, CD44, ErbB signaling, and β-amyloid processing and

Figure 5. **Jagged1 is a TGF-β target that regulates p21 induction and epithelial cytostasis.** (A) Diagram of the signaling pathway established in this paper (black arrows). Gray arrows point to previously established regulatory connections between components of the pathway. Inhibitory connections with compounds and siRNAs at the bottom illustrate the experimental means used during this study. TβR, TGF-β receptor; LY, TGF-β receptor type I inhibitor LY580276; KO, knockout. (B) Quantitative RT-PCR analysis of endogenous *JAGGED1* (*JAG1*) mRNA levels normalized over endogenous *GAPDH* from HaCaT cells transiently transfected with *siLuc* (black lines) or *siJAG1* (gray lines) and subsequently stimulated with 2 ng/ml TGF-β1 for 0, 2, 6, 12, and 24 h. (C) Immunoblot of endogenous JAG1, phospho-Smad2, phospho-Smad3, total Smad2 and Smad3, and α-tubulin control from HaCaT cells transfected as in B and stimulated with 2 ng/ml TGF-β1 for the indicated time points. (D) Quantitative RT-PCR analysis of endogenous *p21* (*CDKN1A*) mRNA levels normalized over endogenous *GAPDH* from HaCaT cells transfected and stimulated as in B. (E) Immunoblot of endogenous p21 and β-tubulin control from HaCaT cells transfected as in B and stimulated with 2 ng/ml TGF-β1 for the indicated time points. (F) Thymidine incorporation assay in HaCaT cells transfected as in B and stimulated with vehicle (gray bars) or 2 ng/ml TGF-β1 (black bars) for 60 h. Error bars represent SD.
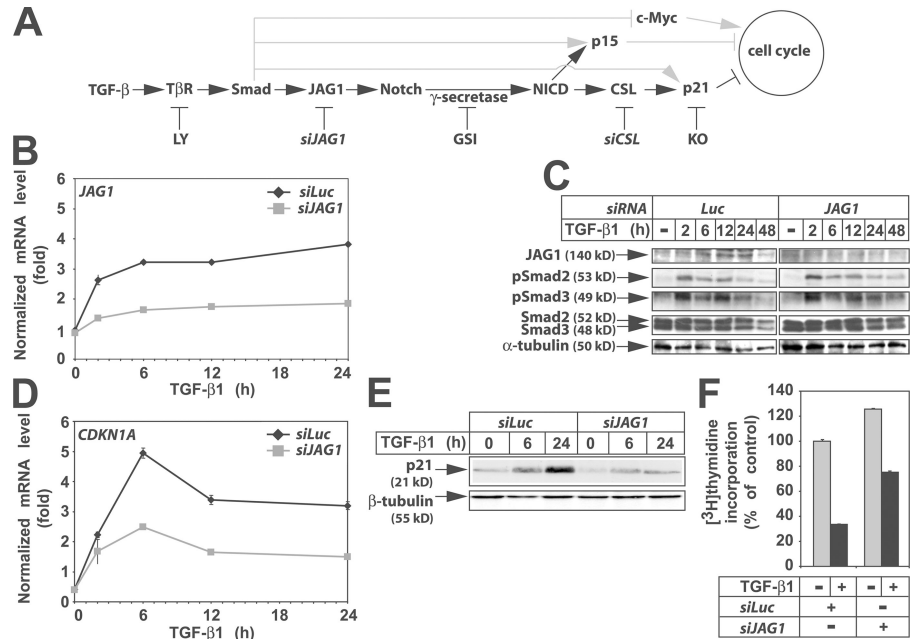
deposition in Alzheimer's disease (Brunkan and Goate, 2005). TGF-β did not appreciably affect the expression or activation of CD44 and ErbB2 in our cell models nor did ligands for these receptors show cooperation with TGF-β–induced cytostasis (unpublished data). More convincingly, the similarity of cellular phenotypes with respect to *p21* gene regulation and keratinocyte proliferation arrest obtained after the use of GSI and knockdown of endogenous *JAG1* and *CSL* after siRNA transfection strongly enforces the model that Notch signaling operates downstream of TGF-β during epithelial cell growth inhibition (Fig. 5 A). During the course of all of the previous experiments, we also monitored the influence of Notch pathway inhibition on the primary activation step of Smad signaling, namely the TGF-β receptor–mediated phosphorylation of Smad2 and Smad3. As previously presented, the knockdown of JAG1 or CSL did not appreciably perturb the normal flow of TGF-β receptor signaling as monitored by phospho-Smad protein levels in extensive time course experiments (Figs. 5 B and 6 B).

In contrast, when the same experiment was repeated after the stimulation of HaCaT cells with TGF-β1 in the presence of GSI, we could observe a partial but considerable inhibition of both phospho-Smad2 and -Smad3 levels (Fig. 7 A). The negative and adverse effects of GSI on phospho-Smad levels was evident throughout extensive time course experiments and was more prominent after 2 h of stimulation with TGF-β1. To test whether activated Notch signaling led to the opposite effect, namely the induction of phospho-Smad levels in HaCaT cells, we infected cells with mock (Ad-GFP) or specific (Ad-N1ICD) adenoviruses and measured phospho-Smad2/3 (Fig. 7 B). Although TGF-β1 induced robust phospho-Smad2 and -Smad3

levels in HaCaT cells, in the presence of control (Ad-GFP) or Ad-N1ICD adenovirus, N1ICD by itself failed to induce phospho-Smad levels. Furthermore, TGF-β1 stimulation of cells expressing ectopic N1ICD did not lead to any further increase of phospho-Smad levels compared with TGF-β1 stimulation alone (Fig. 7 B). Therefore, we conclude that Notch signaling does not seem to contribute to R-Smad phosphorylation by TGF-β receptors in HaCaT cells. However, the use of GSI demonstrates that γ-secretase activity is linked to the process of R-Smad phosphorylation by TGF-β receptors via as yet unknown mechanisms.

The aforementioned result on a potential role of γ-secretase during R-Smad activation obliged us to test even more rigorously the specificity of the observed effects of GSI on *p21* gene induction and epithelial cytostasis downstream of TGF-β. If the GSI effect was primarily caused by the reduction on phospho-Smad levels, Notch should not be able to rescue such effects when provided ectopically. Upon control Ad-GFP infection, TGF-β1 induced endogenous p21 protein levels, and GSI partially blocked this response (Fig. 7 C) as described for uninfected cells (Fig. 4 C). Under such conditions, we also verified that p21 protein induction by TGF-β1 could be enhanced by ectopic N1ICD (Fig. 7 C), confirming a cooperative role of TGF-β1 and Notch1 signaling in maintaining high p21 protein levels. Furthermore, the rescue of p21 expression could be achieved by ectopic N1ICD in a dose-dependent manner (Fig. 7 C). The 3.8-fold inhibition elicited by GSI became 1.3-fold when GSI was combined with a high dose of N1ICD, confirming that GSI primarily blocks endogenous Notch signaling during p21 regulation.
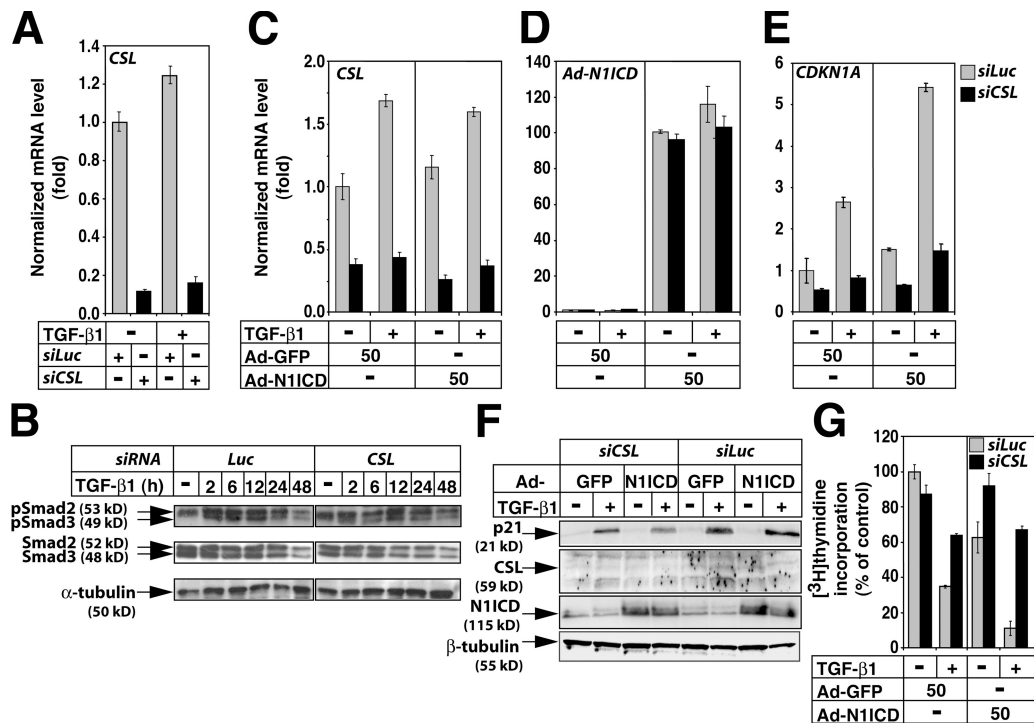
Figure 6. **CSL signaling is critical for p21 induction and epithelial growth arrest by TGF-β.** (A) Quantitative RT-PCR of *CSL* mRNA levels in HaCaT cells transfected with control *siLuc* or specific *siCSL* siRNAs and stimulated or unstimulated with 2 ng/ml TGF-β1 for 16 h. (B) Immunoblot of endogenous phospho-Smad2, phospho-Smad3, total Smad2 and Smad3, and endogenous control α-tubulin levels from HaCaT cells transiently transfected with *siCSL* or *siLuc* before stimulation with 2 ng/ml TGF-β1 for the indicated time points. (C–E) Quantitative RT-PCR analysis of *CSL*, ectopic *Ad-N1ICD*, and *p21* (*CDKN1A*) mRNA normalized over *GAPDH* in HaCaT cells transfected with *siLuc* or *siCSL* and subsequently infected with Ad-GFP or Ad-N1ICD (MOI of 50) before stimulation with 2 ng/ml TGF-β1 for 24 h. (F) Immunoblot of endogenous p21 and CSL, ectopic Ad-N1ICD, and endogenous control β-tubulin levels from HaCaT cells transiently transfected with *siCSL* or *siLuc* and subsequently infected with Ad-GFP or Ad-N1ICD (MOI of 50) before stimulation with 2 ng/ml TGF-β1 for 24 h. The conditions are identical to those in C–E. (G) Thymidine incorporation assay in HaCaT cells transfected with siRNAs as in C, which were subsequently coinfected with the indicated adenoviruses (MOI of 50) and were stimulated or unstimulated with 2 ng/ml TGF-β1 for 60 h. Error bars represent SD.

Similar to these rescue experiments of p21 induction, thymidine incorporation assays confirmed our conclusion about a major role of GSI as a Notch pathway inhibitor (Fig. 7 D). Accordingly, upon control Ad-GFP infection, TGF-β1 inhibited S-phase entry, and GSI reversed this effect (Fig. 7 D). Dose-dependent Ad-N1ICD infection reduced cell growth and, combined with TGF-β1, suppressed growth by 98% (Fig. 7 D). Under these conditions, GSI could weakly restore cell growth, and the higher the N1ICD dose, the less effective GSI was. Thus, N1ICD can antagonize GSI, suggesting that the Notch pathway is a primary target of GSI in the cell model used.

It follows from the model we present in Fig. 5 A that if p21 induction and epithelial cytostasis by TGF-β requires downstream activation of Notch signaling and because JAG1 protein levels accumulate after 6 h of stimulation with TGF-β1 (Fig. 5 B), the addition of GSI in HaCaT cells that are pre-stimulated with TGF-β1 should effectively block the cytostatic response. In all previous experiments, GSI was added 0.5–1 h before TGF-β1 (Fig. 1). However, also when GSI was added 12–18 h after TGF-β1 stimulation, it was effective in blocking the cytostatic response of TGF-β1 weakly by 20–30%, whereas addition between 24 and 48 h gradually enhanced the potency of TGF-β1 in causing cytostasis (Fig. 7 E). Thus, a time window for TGF-β1 cytostasis spans the first 24 h. On the other

hand, the addition of GSI 12–48 h after TGF-β1 could not considerably block p21 protein induction (Fig. 7 F). Thus, robust levels of p21 correspond to the even weak (20%) suppression of thymidine incorporation observed when GSI is added 12 h after TGF-β1 (Fig. 7, E and F; GSI 48 h). This implies that the early period of 0–12 h of TGF-β stimulation represents a critical window during which both p21 induction and suppression of S-phase entry is sensitive to GSI. The small difference observed between the effect of GSI on p21 expression (Fig. 7 F) and thymidine incorporation (Fig. 7 E) when added after TGF-β stimulation emphasizes the role of additional cytostatic regulators such as p15, S100A11, and Id2, which are coregulated by TGF-β and Notch, or c-Myc, which is not regulated by Notch (Fig. 4). Thus, we conclude that GSI primarily acts as an inhibitor of the Notch pathway, and its adverse effect on the accumulation of phosphorylated R- Smads cannot fully explain the cellular phenotypes under investigation.

p21 expression is a critical factor during epithelial cytostasis by TGF-β–Notch

The data support a model whereby TGF-β induces Notch ligands that activate signaling. This supports the duration of TGF-β signaling at sufficiently high and long levels for cell cycle arrest to occur (Fig. 5 A). The induction of JAG1 (and possibly
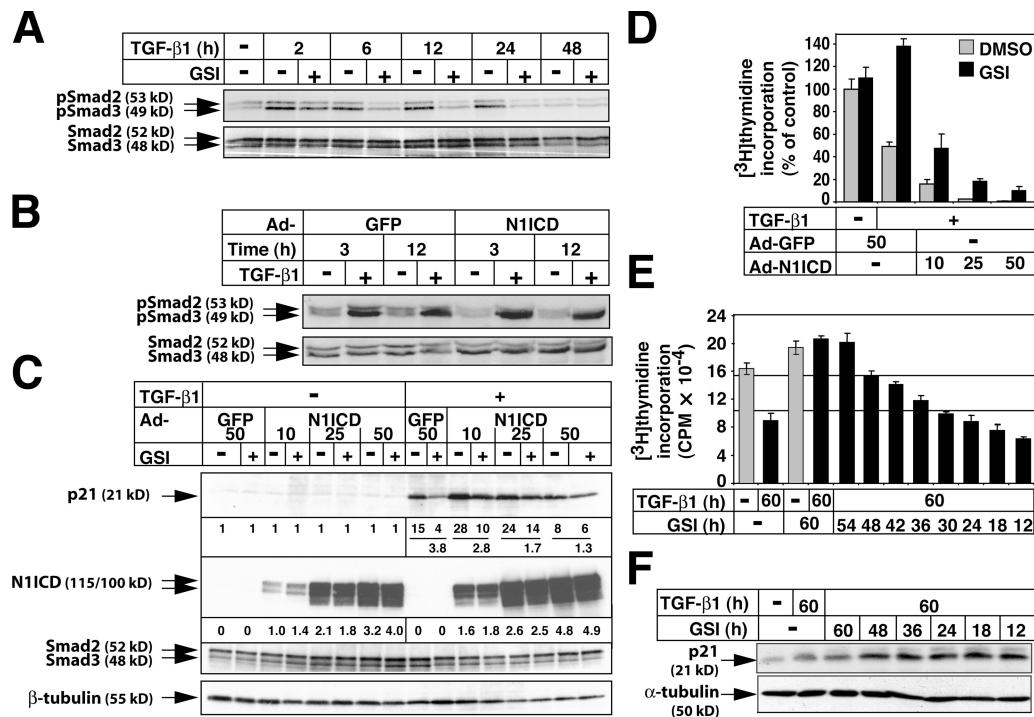
A

TGF-β1 (h)	−	2		6		12		24		48	
GSI	−	−	+	−	+	−	+	−	+	−	+

pSmad2 (53 kD)
pSmad3 (49 kD)

Smad2 (52 kD)
Smad3 (48 kD)

B

Ad-		GFP			N1ICD		
Time (h)		3		12		3	12
TGF-β1	−	+	−	+	−	+	−	+

pSmad2 (53 kD)
pSmad3 (49 kD)

Smad2 (52 kD)
Smad3 (48 kD)

C

TGF-β1				−									+					
Ad-	GFP 50		10		N1ICD 25		50		GFP 50		10		N1ICD 25		50	
GSI	−	+	−	+	−	+	−	+	−	+	−	+	−	+	−	+

p21 (21 kD)

1 1 1 1 1 1 1 1   15 4 28 10 24 14 8 6
                          3.8   2.8   1.7   1.3

N1ICD (115/100 kD)

0 0 1.0 1.4 2.1 1.8 3.2 4.0   0 0 1.6 1.8 2.6 2.5 4.8 4.9

Smad2 (52 kD)
Smad3 (48 kD)

β-tubulin (55 kD)

D

[³H]thymidine incorporation (% of control)

TGF-β1	−	+			
Ad-GFP	50	−			
Ad-N1ICD	−	10	25	50	

(DMSO / GSI)

E

[³H]thymidine incorporation (CPM × 10⁻⁴)

TGF-β1 (h)	−	60	−	60							60		
GSI (h)	−		60	54	48	42	36	30	24	18	12		

F

TGF-β1 (h)	−	60			60			
GSI (h)	−		60	48	36	24	18	12

p21 (21 kD)

α-tubulin (50 kD)

Figure 7. **Role of γ-secretase on the accumulation of phospho-Smad levels.** (A) Immunoblot of endogenous phospho-Smad2 and -Smad3 and corresponding total Smad2 and Smad3 levels in HaCaT cells stimulated with 2 ng/ml TGF-β1 for the indicated time points in the presence of DMSO (−) or 4 μM GSI (+). (B) Immunoblot of endogenous phospho-Smad2 and -Smad3 and corresponding total Smad2 and Smad3 levels in HaCaT cells transiently infected with Ad-GFP or Ad-N1ICD (MOI of 50 each) before stimulation with 2 ng/ml TGF-β1 for the indicated time points. (C) Immunoblot of p21, ectopic N1ICD, and control Smad2/Smad3 and β-tubulin from HaCaT cells infected with Ad-GFP (MOI of 50) or Ad-N1ICD (MOI of 10, 25, and 50) before stimulation with 2 ng/ml TGF-β1 for 24 h in the absence (−, DMSO) or presence (+) of 4 μM GSI. Densitometric values of p21 protein bands normalized over β-tubulin are shown between the immunoblots. The 0-h TGF-β1 without GSI condition is normalized to 1.0, and all other values are expressed relatively. In the right panel, the denominator represents the fold decrease in inducible p21 caused by GSI. (D) Thymidine incorporation assays in HaCaT cells infected with Ad-GFP or Ad-N1ICD (MOI of 10, 25, and 50) and stimulated with vehicle (−) or 2 ng/ml TGF-β1 (+) for 60 h in the absence (DMSO) or presence of 4 μM GSI. (E) Thymidine incorporation assay in HaCaT cells stimulated with 2 ng/ml TGF-β1 for 60 h in the absence or presence of 4 μM GSI, which was added after the onset of TGF-β1 stimulation and was present in the cell culture for the indicated time points. The top horizontal line indicates the level of thymidine incorporation that corresponds to 80% of the control level in the presence of GSI (third bar), and the bottom horizontal line corresponds to the level of thymidine incorporation that shows a statistically significant (P < 0.05) difference from the level of thymidine incorporation in the presence of TGF-β1 in the control condition (second bar). All values below this line are not significantly different from this reference point (P < 0.05) except for the last condition, which is significantly lower. (F) Immunoblot of endogenous p21 and α-tubulin control from HaCaT cells stimulated with 2 ng/ml TGF-β1 for 60 h in the absence or presence of 4 μM GSI that was added after TGF-β1 stimulation and stayed in the culture for the indicated time points. The conditions are identical to those in E. Error bars represent SD.

DLL4) by TGF-β leads to the activation of endogenous Notch/CSL signaling, which is required for sustained p21 induction and is important for epithelial cytostasis by TGF-β. The latter conclusion was verified after ectopic p21 expression (Fig. S3, available at http://www.jcb.org/cgi/content/full/jcb.200612129/DC1), which antagonized the reversion in TGF-β1–mediated growth arrest elicited by GSI and led to robust cytostasis (Fig. S3 A). Interestingly, very high levels of ectopic p21 protein (6–10-fold relative to the endogenous TGF-β–induced p21 level) were required to bypass the neutralizing effect of GSI (Fig. S3 B). This suggests that TGF-β in the presence of GSI might induce target genes that permit sustained cell proliferation even in the presence of high levels of potent cell cycle inhibitors such as p21. This finding plus the previous result on p21 induction by TGF-β1 in the presence of GSI that was added several hours after TGF-β1 (Fig. 7 F) raised the possibility that although *p21* clearly is a responsive gene to the TGF-β–Notch pathways, the physiological relevance of p21 to epithelial cytostasis induced by the same pathways remains to be determined.

To rigorously test the role of p21 on epithelial cytostasis downstream of TGF-β–Notch signaling, we attempted to knock-down p21 expression in HaCaT cells after siRNA transfection. Such attempts always led to a partial reduction of p21 mRNA and protein levels by 60–70%, which correlated with a partial defect in the cytostatic response to TGF-β (unpublished data). To obtain definitive evidence for a role of p21 in the TGF-β cytostatic program, we made use of two individual cell clones of human mammary epithelial MCF-10A cells, whose endogenous *p21* gene was deleted after homologous recombination (Fig. 8 and Fig. S4, available at http://www.jcb.org/cgi/content/full/jcb.200612129/DC1; Bachman et al., 2004). Similar to the effect on HaCaT, NMuMG, and HMEC cells (Figs. 1 and S1), TGF-β1 suppressed thymidine incorporation in control uninfected MCF-10A cells (unpublished data) or in MCF-10A cells transiently infected with control Ad-GFP (Fig. 8 A). Ad-N1ICD infection led to a substantial suppression of S-phase entry, which was comparable with that obtained by 2 ng/ml TGF-β1 (Fig. 8 A). The combination of TGF-β1 and N1ICD led to a
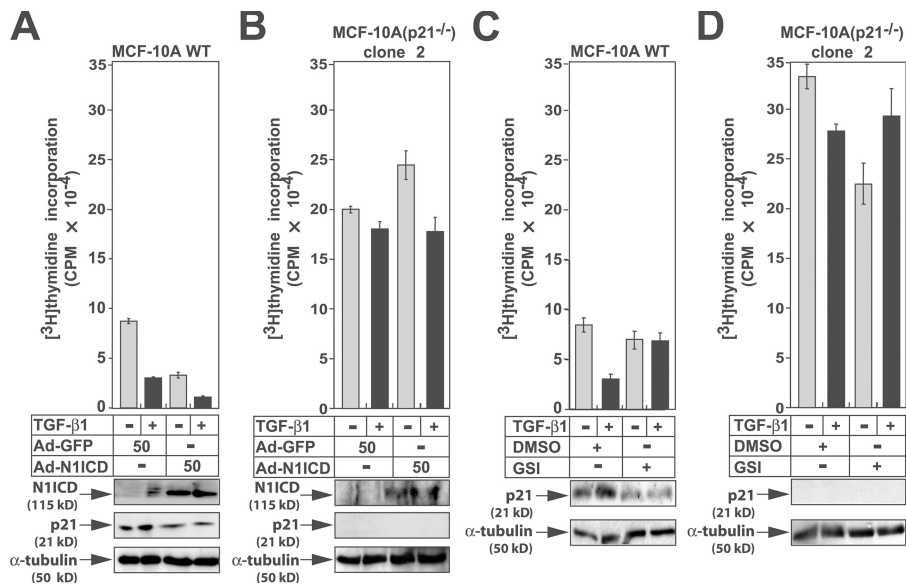
Figure 8. **The cell cycle inhibitor p21 is required for mammary epithelial cytostasis by TGF-β and Notch.** (A–D) Thymidine incorporation assays in MCF-10A wild-type (WT) cells (A and C) or MCF-10A p21$^{-/-}$ homozygous knockout clone 2 cells (B and D) infected with Ad-GFP or Ad-N1ICD (MOI of 50) and either stimulated with vehicle (−) or 2 ng/ml TGF-β1 for 60 h (A and B) or stimulated with TGF-β1 in the presence or absence of 4 μM GSI (C and D). Immunoblots from the same cells for ectopic N1ICD, endogenous p21, and control endogenous α-tubulin are shown below the bar graphs. Error bars represent SD.

very strong cytostatic response (Fig. 8 A). In contrast, infection of the p21 knockout clones of MCF-10A cells and stimulation with TGF-β1 failed to show any measurable suppression of thymidine incorporation (Figs. 8 B and S4 A). The reciprocal experiment using GSI as a means of blocking endogenous Notch signaling corroborated the results with ectopic N1ICD expression. Thus, GSI effectively blocked the suppression of thymidine incorporation by TGF-β1 in wild-type MCF-10A (Fig. 8 C), whereas in the p21 knockout clones, thymidine levels remained high in the absence or presence of GSI (Figs. 8 D and S4 B). It is worth noting that the two p21 knockout clones incorporated substantially higher levels of thymidine compared with wild-type cells (Figs. 8 and S4). This correlated well with the absence and presence of endogenous p21 protein expression, respectively (Fig. 8, bottom; and Fig. S4 C). Therefore, these experiments strongly implicate a functional role of p21 in the cytostatic response of epithelial cells downstream of TGF-β and Notch signaling.

Discussion

The impetus for this study was the realization that TGF-β and Notch pathways act as tumor suppressor and prometastatic or oncogenic pathways during carcinogenesis (Radtke and Raj, 2003; Pardali and Moustakas, 2007). We establish that Notch and TGF-β cooperatively suppress epithelial cell growth when both pathways are simultaneously activated. On the other hand, TGF-β induces Jagged1 ligand synthesis, which then activates Notch signaling in the same cell population, thus rendering TGF-β partially dependent on Notch signaling during the establishment of cytostasis (Figs. 1, 3, and 5). We observed the same type of interdependent relationship between the two pathways when large-scale gene expression analysis was performed (Figs. 2 and 4). Additionally, however, we measured many genes that were uniquely regulated by the combined input of TGF-β1 and Notch1 both positively and negatively. Finally, we demonstrate that TGF-β–induced cytostasis requires the durable

expression of factors such as p21, which is achieved by an initial TGF-β input followed by a secondary but indispensable Notch input (Figs. 5 and 6). While p21 is not the only gene of the cytostatic program of TGF-β that is affected by Notch signaling inhibition, evidence derived from p21 knockout epithelial cells strongly links this cell cycle regulator to the cytostatic response of the cells. Analyzing in detail the functional roles of other genes uncovered in this study and the detailed mechanisms of their regulation by TGF-β and Notch may shed light on even more novel facets of the binary roles these two pathways play during the control of epithelial proliferation and tumor development.

In analyzing the transcriptomic response of HaCaT keratinocytes to TGF-β in the presence of GSI (Figs. 2 and 4), we uncovered an extensive dependence of gene expression regulation on endogenous Notch pathway activation. Based on careful control experiments in which we examined the role of GSI on phospho-Smad accumulation in response to TGF-β (Fig. 7 A), two possible working models can explain the transcriptomic results. First, an adverse negative effect of GSI on phospho-Smad accumulation may be the main reason behind the substantial decrease in the number of TGF-β–responsive genes we measured, especially at the 6-h time point (Fig. 2 A). In simple terms, GSI lowers the active levels of Smads in the epithelial cell, thus reducing the downstream output of these signal transducers as measured by gene expression readouts. However, the majority of the evidence presented here argues against this model. Two examples are illustrative: (1) a large number of new target genes of the TGF-β pathway were uncovered in our screen whose expression is regulated only when cells are treated with GSI (Fig. 2 B and Table S1). This suggests that the inhibition of γ-secretase activity in the cell redirects the specificity of gene expression regulation by TGF-β toward new targets. This phenomenon is hard to reconcile based on a model in which Smad activation is gradually diminishing as a result of GSI. (2) Specific gene targets of TGF-β/Smad signaling such as TIEG (Fig. 2 C) or c-Myc (Fig. 4 B) are not affected at all by the presence of GSI. If the inhibitor

were simply reducing phospho-Smad levels, these two and other genes should have shown new expression profiles in the presence of GSI, which was never observed.

The second working model, which is corroborated by the majority of the data presented here, is outlined in Fig. 5 A and essentially favors a sequential mode of signaling starting with TGF-β and later followed by Notch. This pathway targets critical mediators of the cytostatic response of epithelial cells, namely the cell cycle inhibitors p15 and p21. Depletion of endogenous Jagged1 and CSL proteins supports this model, and no evidence for a contribution of these classic Notch pathway components to the process of Smad activation could be gained (Figs. 5 and 6). This model of sequential signaling suggests that gene targets like p15 and p21 are directly regulated by the incoming Smad pathway as previously established (Feng et al., 2000; Pardali et al., 2000, 2005; Seoane et al., 2001, 2004; Gomis et al., 2006b), and subsequent onset of Notch signaling after the accumulation of ligands of this pathway, such as Jagged1, contributes to a sustained and robust transcriptional induction of the same genes. From this perspective, it would be interesting to examine in deeper detail the transcriptional mechanisms that mediate the regulation of p15 and p21 gene expression by the combined TGF-β/Smad and Notch/CSL signaling inputs. In this respect, it is interesting that Jagged1 clusters together with p15 and p21 as genes of the same synexpression group downstream of TGF-β, as all of these genes seem to require the activity of Smad signaling and the cooperation of transcription factors of the FoxO family (Gomis et al., 2006a). The mechanistic details of how Smads, FoxO members, and additional cofactors orchestrate the time-dependent induction of Jagged1 remain to be elucidated.

An interesting question remaining open at this stage is the mechanism by which the inhibition of γ-secretase affects the accumulation of phosphorylated R-Smads downstream of the TGF-β receptor. Presently, we examine three alternative possibilities: (1) γ-secretase may be involved in the activation process of the TGF-β receptor, thus playing a critical role in the phosphorylation of R-Smads by the type I receptor; (2) γ-secretase positively contributes to the stability of phosphorylated R-Smads, possibly by down-regulating an ubiquitin ligase involved in phosphorylated R-Smad turnover; or (3) γ-secretase negatively regulates the phosphatases that remove the C-terminal phosphates from phospho–R-Smads. Ongoing work aims at addressing these alternative mechanisms.

Among all components of the Notch pathway whose expression is regulated by TGF-β signaling, our evidence favors more prominent roles for the ligands of these pathways such as Jagged1 and DLL4 in keratinocytes (Fig. 3 B) or Jagged1 and DLL1 in mammary epithelial cells (Fig. S2). The observed regulation of receptors of the Notch pathway appeared to be indirect (unpublished data) and possibly the result of an autogenous negative feedback pathway whereby the activation of Notch signaling itself leads to the down-regulation of its receptor genes. Although our evidence favors this model, TGF-β was found to up-regulate the expression of Notch4 concomitantly to the down-regulation of Notch1, at least in mammary epithelial cells (Fig. S2). The functional relevance of such a reciprocal regulation of Notch receptors during cytostasis of mammary epithelial

cells remains unknown. Alternatively, TGF-β may instruct for this switch of Notch receptor expression as it promotes epithelial-mesenchymal transition of the mammary cells, a physiological response in which the cross talk between TGF-β and Notch signaling has already been established at least in keratinocytes (Zavadil et al., 2004).

In establishing the sequential signaling pathway of TGF-β followed by Notch as a critical regulator of epithelial cytostasis (Fig. 5 A), we primarily focused on regulation of the cell cycle inhibitor p21. This was prompted by the characteristic expression profile measured for p21 during our experiments (Fig. 4 B). However, regulation of additional factors such as p15, Id2, or S100A11 seems to also be integrated in the same physiological response. Thus, in emphasizing a role of p21 as a major target gene of the sequential signaling cascade outlined here, one should strongly consider the legitimate and equipotent contribution of the other regulators of this multigenic response to TGF-β. This point is underscored by the experiments using p21 knockout MCF-10A cells (Figs. 8 and S4). Our evidence fully recapitulates the original findings of Bachman et al. (2004) and further demonstrates the role of p21 downstream of Notch signaling in mammary epithelial cells. However, it should be kept in mind that MCF-10A cells represent relatively normal immortalized human epithelial cells that have spontaneously lost the expression of their endogenous p15 cell cycle inhibitor gene (Chen et al., 2001). Thus, the p21 knockout MCF-10A clones represent a double knockout for p15 and p21 expression, and this is the main reason why TGF-β completely fails to elicit proliferation arrest in these cell clones. Our attempts to deplete p15 or p21 individually from HaCaT or other epithelial cell models in which TGF-β–mediated cytostasis is well understood always led to partial and relatively weak phenotypes, presumably because of the compensation provided by the other genes of the cytostatic program that remained intact (unpublished data).

In summary, this study establishes a relay mechanism of signal transduction that plays critical roles for the establishment of epithelial cell cycle arrest. This mechanism fits well with the established tumor suppressor roles of TGF-β and Notch signaling. Additionally, this mechanism opens the exciting possibility whereby the two signaling pathways may be misregulated in an interdependent manner during human tumor progression, thus offering a promising territory for future studies in cancer cell biology.

Materials and methods

Cells and reagents

Human HaCaT keratinocytes, human MCF-10A mammary epithelial cells, human embryonic kidney 293 cells, mouse NMuMG mammary epithelial cells, and their derivative clone NMe have been described previously (Valcourt et al., 2005). Mink lung epithelial cells (Mv1Lu) were purchased from the American Type Culture Collection, and HMECs were obtained from R.A. Weinberg (Whitehead Institute for Biomedical Research/Massachusetts Institute of Technology, Cambridge, MA). MCF-10A clones 1 and 2 deficient in the endogenous *p21* gene were obtained from B.H. Park (The Sidney Kimmel Comprehensive Cancer Center at Johns Hopkins University, Baltimore, MD; Bachman et al., 2004). Recombinant mature TGF-β1 was purchased from PeproTech. The TGF-β type I receptor kinase inhibitor LY580276 and TGF-β types I and II receptor kinase dual inhibitor LY364947 were obtained from J.M. Yingling (Eli Lilly, Inc., Indianapolis, IN; Peng et al., 2005). The inhibitor X against γ-secretase activity (GSI) was purchased from Merck Biosciences/Calbiochem.

Transient adenoviral infections and siRNA transfections

Adenoviruses expressing GFP were based on the bicistronic Adeasy vector obtained from B. Vogelstein (The Johns Hopkins Medical Institutions, Baltimore, MD). Adenoviruses expressing N1ICD were based on Adeasy, which was obtained from G.P. Dotto (Harvard Medical School, Boston, MA) and F. Radtke (Ludwig Institute for Cancer Research [LICR], Lausanne, Switzerland). Adenoviruses expressing wild-type human p21 were obtained from K. Walsh (Boston University School of Medicine, Boston, MA). Adenoviruses were amplified and titrated in human embryonic kidney 293 cells, and transient infections were performed as described previously (Valcourt et al., 2005). Under standardized conditions, epithelial cells were infected at a rate of 75–85% without any signs of cytotoxicity as assessed by live GFP autofluorescence and immunofluorescence microscopy.

The human *CSL*-specific (GenBank/EMBL/DDBJ accession no. NM_005348; reagent number M-007772; human RBPSUH) and human *JAG1*-specific (GenBank/EMBL/DDBJ accession no. NM_000214; reagent number L-011060; human Jag1) siRNAs were pools of four RNA oligonucleotides termed On-Target Plus SMARTpools that minimize off-target effects; siRNA against the *luciferase* reporter vector pGL2 (GenBank/EMBL/DDBJ accession no. X65324) served as a control. All siRNAs were purchased from Dharmacon. HaCaT cells were transiently transfected with 20 nM siRNA using siLentFect (Bio-Rad Laboratories) according to the manufacturer's protocol. Cells were transfected 1 d after seeding, remained with transfection cocktail for 24 h, were switched to fresh medium plus TGF-β1, and were retransfected with siRNA for another 24 h before cell analysis.

Immunoblotting

Total proteins from NMuMG or HaCaT cells were extracted, subjected to SDS-PAGE, and analyzed by Western blotting as described previously (Valcourt et al., 2005). Mouse monoclonal anti–β-tubulin (T8535) antibody was obtained from Sigma-Aldrich; mouse monoclonal anti-Cip1/WAF1 (clone 70) was purchased from BD Transduction Laboratories; rabbit polyclonal anti-Notch1 (ab8925) was purchased from Abcam; mouse monoclonal anti-Smad1/2/3 (H2), rabbit polyclonal anti-Notch4 (H-225), rabbit polyclonal anti-Notch3 (M-134), rabbit polyclonal anti-Jagged1 (H-66), rabbit polyclonal anti-TGFβRI (V-22), rabbit anti-CSL/RBP-Jκ, rabbit anti-DLL4/Delta-4 (H-70), and mouse anti–α-tubulin (TU-02) were obtained from Santa Cruz Biotechnology, Inc. Secondary anti–mouse IgG and anti–rabbit IgG coupled to HRP were obtained from GE Healthcare. The ECL detection system was prepared in house, and immunoblots were scanned on a CCD camera (LAS-1000; Fuji). Densitometry was performed using the AIDA program of the scanner.

Thymidine incorporation, cell counting, and FACS assays

Cells were cultured, stimulated with growth factors, and labeled metabolically with [³H]thymidine as described previously (Valcourt et al., 2005). The data are plotted as mean values with SEMs of triplicate repeats per independent experiment. Each independent experiment was repeated at least three times. Cell monolayers were washed with PBS, trypsinized, and stained with trypan blue (Sigma-Aldrich), and viable cell numbers were calculated using a counter (Z1; Beckman Coulter). Cell numbers are plotted as means from triplicate determinations with SEMs per experiment.

For FACS analysis of cell cycle distribution, cells were trypsinized and resuspended in ice-cold PBS/10 mM EDTA, centrifuged for 5 min at 2,500 rpm and 4°C, resuspended in PBS/0.1% wt/vol glucose, fixed in −20°C-cold 70% vol/vol ethanol, washed in PBS/10 mM EDTA twice, and stained with 0.1 mg/ml propidium iodine by coincubation with RNAase. Stained cells were analyzed in a Guava EasyCyte Mini System (Guava Technologies, Inc.) according to the manufacturer's protocol and built-in software. Mean cell number per cell cycle phase was estimated based on measurements from 5,000 cells per single reading. The data are plotted in bar graphs representing percentiles of the total cell population.

Statistical analysis

Statistical analysis of thymidine incorporation assays was performed by two-tailed paired *t* tests. Significance was considered at a p-value of <0.05.

cDNA microarray analysis

HaCaT cells were cultured in the presence of 3% FBS and stimulated with 2 ng/ml TGF-β1 for 2, 6, and 48 h in the absence or presence of 4 μM GSI. Cells for the 2-h time point were also incubated with 10 μg/ml cycloheximide to block protein synthesis. Total RNA extraction and cDNA probe labeling was performed as described previously (Valcourt et al., 2005). Equal amounts of labeled cDNA probes per pair were hybridized to cDNA microarray chips (Hver2.1.1) from the Sanger/LICR/Cancer Research UK Consortium (see http://www.sanger.ac.uk/Projects/Microarrays/ for details and hybridization protocols). The glass chips contained 14,633 single-stranded cDNA elements of 1.5-kb mean length, which represent 10,252 unique human genes. The human IMAGE cDNA clone collection was obtained from the Medical Research Council Human Genome Microarray Platform Resource Centre. cDNA clone resequencing was performed by Team 56 at the Sanger Institute. Hybridizations were performed in triplicate using RNAs from three independent cultures and including the dye swap control. Microarray scanning, image analysis, and primary spot intensity statistical analysis were performed as described previously (Valcourt et al., 2005). Regulated genes were selected based on the mean ratio value of ≥1.7 for up-regulated genes and ≤0.55 for down-regulated genes. In addition, regulated genes had to be expressed on three arrays out of three and with a *t* test value for the ratios within replicates corresponding to a probability of <0.05. Statistically significant genes (P < 0.05) were clustered based on their expression values using the K-means statistical algorithm that is incorporated into GeneSpring 7.2 data mining software (Silicon Genetics/Agilent Technologies). For all time points, we considered as a reference a duplicate cell culture in which TGF-β1 was replaced by vehicle. Functional classification of regulated genes was performed manually based on exhaustive PubMed searches (http://www.ncbi.nlm.nih.gov/PubMed/).

Semiquantitative RT-PCR and quantitative real-time RT-PCR

Total RNA from NMuMG or HaCaT cells was analyzed by semiquantitative RT-PCR as described previously (Valcourt et al., 2005) using specific primers (Table I). Primers for mouse *glyceraldehyde-3′-phosphate dehydrogenase* (*Gapdh*) were used to ascertain that an equivalent amount of cDNA was synthesized. Specificity controls included reactions in which reverse transcriptase was omitted (−RT) and in which cDNAs were replaced with water.

DNase RQI–digested RNA from NMuMG and HaCaT cells was analyzed by quantitative real-time RT-PCR as described previously (Valcourt et al., 2005). Primers (Table I) were designed with Primer Express (Applied Biosystems). Reactions were performed in a sequence detector (ABI-Prism 7000; Applied Biosystems) in triplicate, and, for each condition, the ground condition (minus TGF-β1 and/or mock infected with Ad-GFP) was set as 1; expression data are presented as bar graphs of mean values plus SD.

Online supplemental material

Fig. S1 shows thymidine incorporation and cell counting assays in various epithelial cell types. Fig. S2 shows semiquantitative RT-PCR assays and corresponding immunoblot assays for Notch family member expression in NMuMG cells. Fig. S3 shows thymidine incorporation and immunoblot assays in HaCaT cells expressing ectopic p21. Fig. S4 shows thymidine incorporation and immunoblot data from clone 1 of the p21 knockout MCF-10A cells. Table S1 provides information about transcriptomic analysis of the TGF-β1 response after Notch inhibition.Online supplemental material is available at http://www.jcb.org/cgi/content/full/jcb.200612129/DC1.

Table I. **Oligonucleotide primers used for RT-PCR analyses**

Gene	Primer sequence (strand)	Product size	Temperature	PCR cycle	Accession no. or reference
		bp	℃		
Notch1	5′-CAGAACTTACAGCTCCAGCC-3′ (+)	458	58	28	NM_008714
	5′-CCTCTGGAATGTGGGTGATC-3′ (−)				
Notch4	5′-CAAGTTGCCTGGGGTCTTCC-3′ (+)	458	60	32	NM_010929
	5′-GGCAAGGAGTCATCAGCTGG-3′ (−)				
Jagged1	5′-CAGTGGCTTGGGTCTGTTGC-3′ (+)	321	58	30	NM_013822
	5′-CCTTCTCCTCTCTGTCTACC-3′ (−)				
Jagged2	5′-GAGTTCCAGTGTGACGCCTA-3′ (+)	457	58	32	NM_010588
	5′-GGGCCTCGTGAATATGACCA-3′ (−)				
Dll1	5′-CATCATTGGGGCTACCCAGA-3′ (+)	482	58	36	NM_007865
	5′-CCTGAACCTGGTTCTCAGCA-3′ (−)				
Gapdh	5′-ATCACTGCCACCCAGAAGAC-3′ (+)	443	57	26	Valcourt et al., 2005
	5′-ATGAGGTCCACCACCCTGTT-3′ (−)				
CCNB2	5′-CCCACCAAAACAACAAATGTCA-3′ (+)	150	60	qPCR	ENSG00000157456/ AY864066
	5′-CATCAGAAAAAGCTTGGCAGAGA-3′ (−)				
CDKN1A	5′-CTGCCCAAGCTCTACCTTCC-3′ (+)	123	60	qPCR	Pardali et al., 2005
	5′-CAGGTCCACATGGTCTTCCT-3′ (−)				
CDKN2B	5′-TGGACCTGGTGGCTACGAAT-3′ (+)	150	60	qPCR	OTTHUMG 00000019691
	5′-AGGGCCTAAGTTGTGGGTTCA-3′ (−)				
CSL	5′-AGGTAATTTCATGCCAGTTCACA-3′ (+)	150	60	qPCR	ENSG00000168214
	5′-CATGCCAGTAACTGAGCACACA-3′ (−)				
DLL1	5′-TGAGGTGTAAAATGGAAGTGAGATG-3′ (+)	151	60	qPCR	ENSG00000198719
	5′-AGAACCTGCTCGGTCTGAACTC-3′ (−)				
DLL3	5′-CCCCGGACCGTCAGT-3′ (+)	151	60	qPCR	ENSG00000090932
	5′-GATGGAAGGAGCAGATATGACATAAAT-3′ (−)				
DLL4	5′-CTTGTGAATGTCCCCCCAACT-3′ (+)	150	60	qPCR	ENSG00000128917
	5′-CAGTAGGTGCCCGTGAATCC-3′ (−)				
GADD45B	5′-GGGAAGGTTTTGGGCTCTCT-3′ (+)	150	60	qPCR	ENSG00000099860/ AF087853
	5′-CGGTCACCGTCCGCATCTT-3′ (−)				
JAG1	5′-GATGATGGGAACCCGATCAA-3′ (+)	150	60	qPCR	ENSG00000101384
	5′-GCAAGGGAACAAGGAAATCTGT-3′ (−)				
JAG2	5′-GACTGCCGCATCAACATG-3′ (+)	232	60	qPCR	ENSG00000184916
	5′-CACCACACCTTGCTGCAGTC-3′ (−)				
N1ICD	5′-CGGGTCCACCAGTTTGAATG-3′ (+)	76	60	qPCR	ENSG00000148400
	5′-GTTGTATTGGTTCGGCACCAT-3′ (−)				
NOTCH1	5′-AAACAAGTGAAAGCATATGGGT-3′ (+)	137	60	qPCR	ENSG00000148400/ NM_017617.2
	5′-CCTGAAACAAAGATTCATGATT-3′ (−)				
NOTCH2	5′-TGTCTTCCAGATTCTGATTCGC-3′ (+)	243	60	qPCR	ENSG00000134250
	5′-GGTGTCTCTTCCTTGTTGTCC-3′ (−)				
NOTCH3	5′-TGATCGGCTCGGTAGTAATGC-3′ (+)	114	60	qPCR	ENSG00000074181
	5′-GACAACGCTCCCAGGTAGTCA-3′ (−)				
NOTCH4	5′-GGAGAGGGTAAAAAATGAAAGAATACATG-3′ (+)	154	60	qPCR	ENSG00000112049
	5′-GGCATACATTCATTTTAGGAGAGAAAC-3′ (−)				
c-MYC	5′-AGGGTCAAGTGGGACAGTGTCA-3′ (+)	150	60	qPCR	ENSG00000136997
	5′-AGCTCCGTTTTAGCTCGTTCCT-3′ (−)				
GAPDH	5′-GGAGTCAACGGATTTGGTCGTA-3′ (+)	78	60	qPCR	ENSG00000111640
	5′-GGCAACAATATCCACTTTACCAGAGT-3′ (−)				

Lowercase gene names refer to mouse sequences, and capitalized gene names refer to human sequences. When quantitative PCR (qPCR) assays are performed, the PCR cycle number is not applicable.

References

Akiyoshi, S., M. Ishii, N. Nemoto, M. Kawabata, H. Aburatani, and K. Miyazono. 2001. Targets of transcriptional regulation by transforming growth factor-β: expression profile analysis using oligonucleotide arrays. *Jpn. J. Cancer Res.* 92:257–268.

Bachman, K.E., B.G. Blair, K. Brenner, A. Bardelli, S. Arena, S. Zhou, J. Hicks, A.M. De Marzo, P. Argani, and B.H. Park. 2004. p21[WAF1/CIP1] mediates the growth response to TGF-β in human epithelial cells. *Cancer Biol. Ther.* 3:221–225.

Blokzijl, A., C. Dahlqvist, E. Reissmann, A. Falk, A. Moliner, U. Lendahl, and C.F. Ibanez. 2003. Cross-talk between the Notch and TGF-β signaling pathways mediated by interaction of the Notch intracellular domain with Smad3. *J. Cell Biol.* 163:723–728.

Brunkan, A.L., and A.M. Goate. 2005. Presenilin function and γ-secretase activity. *J. Neurochem.* 93:769–792.

Chen, C.R., Y. Kang, and J. Massagué. 2001. Defective repression of c-myc in breast cancer cells: a loss at the core of the transforming growth factor β growth arrest program. *Proc. Natl. Acad. Sci. USA*. 98:992–999.

Chen, C.R., Y. Kang, P.M. Siegel, and J. Massagué. 2002. E2F4/5 and p107 as Smad cofactors linking the TGFbeta receptor to c-myc repression. *Cell.* 110:19–32.

Croquelois, A., A. Blindenbacher, L. Terracciano, X. Wang, I. Langer, F. Radtke, and M.H. Heim. 2005. Inducible inactivation of Notch1 causes nodular regenerative hyperplasia in mice. *Hepatology.* 41:487–496.

Feng, X.-H., X. Lin, and R. Derynck. 2000. Smad2, Smad3 and Smad4 co-operate with Sp1 to induce p15^{Ink4B} transcription in response to TGF-β. *EMBO J.* 19:5178–5193.

Gomis, R.R., C. Alarcon, W. He, Q. Wang, J. Seoane, A. Lash, and J. Massagué. 2006a. A FoxO-Smad synexpression group in human keratinocytes. *Proc. Natl. Acad. Sci. USA.* 103:12747–12752.

Gomis, R.R., C. Alarcon, C. Nadal, C. Van Poznak, and J. Massagué. 2006b. C/EBPβ at the core of the TGFβ cytostatic response and its evasion in metastatic breast cancer cells. *Cancer Cell.* 10:203–214.

Itoh, F., S. Itoh, M.J. Goumans, G. Valdimarsdottir, T. Iso, G.P. Dotto, Y. Hamamori, L. Kedes, M. Kato, and P. ten Dijke. 2004. Synergy and antagonism between Notch and BMP receptor signaling pathways in endothelial cells. *EMBO J.* 23:541–551.

Kang, Y., C.R. Chen, and J. Massagué. 2003. A self-enabling TGFβ response coupled to stress signaling. Smad engages stress response factor ATF3 for Id1 repression in epithelial cells. *Mol. Cell.* 11:915–926.

Lai, E.C. 2004. Notch signaling: control of cell communication and cell fate. *Development.* 131:965–973.

Levy, L., and C.S. Hill. 2006. Alterations in components of the TGF-β superfamily signaling pathways in human cancer. *Cytokine Growth Factor Rev.* 17:41–58.

Mammucari, C., A.T. di Vignano, A.A. Sharov, J. Neilson, M.C. Havrda, D.R. Roop, V.A. Botchkarev, G.R. Crabtree, and G.P. Dotto. 2005. Integration of Notch 1 and calcineurin/NFAT signaling pathways in keratinocyte growth and differentiation control. *Dev. Cell.* 8:665–676.

Massagué, J., J. Seoane, and D. Wotton. 2005. Smad transcription factors. *Genes Dev.* 19:2783–2810.

Nicolas, F.J., and C.S. Hill. 2003. Attenuation of the TGF-β-Smad signaling pathway in pancreatic tumor cells confers resistance to TGF-β-induced growth arrest. *Oncogene.* 22:3698–3711.

Nicolas, M., A. Wolfer, K. Raj, J.A. Kummer, P. Mill, M. van Noort, C.C. Hui, H. Clevers, G.P. Dotto, and F. Radtke. 2003. Notch1 functions as a tumor suppressor in mouse skin. *Nat. Genet.* 33:416–421.

Noseda, M., L. Chang, G. McLean, J.E. Grim, B.E. Clurman, L.L. Smith, and A. Karsan. 2004. Notch activation induces endothelial cell cycle arrest and participates in contact inhibition: role of p21^{Cip1} repression. *Mol. Cell. Biol.* 24:8813–8822.

Pardali, K., and A. Moustakas. 2007. Actions of TGF-β as tumor suppressor and pro-metastatic factor in human cancer. *Biochim. Biophys. Acta.* 1775:21–62.

Pardali, K., A. Kurisaki, A. Morén, P. ten Dijke, D. Kardassis, and A. Moustakas. 2000. Role of Smad proteins and transcription factor Sp1 in p21$^{Waf1/Cip1}$ regulation by transforming growth factor-β. *J. Biol. Chem.* 275:29244–29256.

Pardali, K., M. Kowanetz, C.-H. Heldin, and A. Moustakas. 2005. Smad pathway-specific transcriptional regulation of the cell cycle inhibitor p21$^{WAF1/Cip1}$. *J. Cell. Physiol.* 204:260–272.

Peng, S.B., L. Yan, X. Xia, S.A. Watkins, H.B. Brooks, D. Beight, D.K. Herron, M.L. Jones, J.W. Lampe, W.T. McMillen, et al. 2005. Kinetic characterization of novel pyrazole TGF-β receptor I kinase inhibitors and their blockade of the epithelial-mesenchymal transition. *Biochemistry.* 44:2293–2304.

Qi, R., H. An, Y. Yu, M. Zhang, S. Liu, H. Xu, Z. Guo, T. Cheng, and X. Cao. 2003. Notch1 signaling inhibits growth of human hepatocellular carcinoma through induction of cell cycle arrest and apoptosis. *Cancer Res.* 63:8323–8329.

Radtke, F., and K. Raj. 2003. The role of Notch in tumorigenesis: oncogene or tumour suppressor? *Nat. Rev. Cancer.* 3:756–767.

Rangarajan, A., C. Talora, R. Okuyama, M. Nicolas, C. Mammucari, H. Oh, J.C. Aster, S. Krishna, D. Metzger, P. Chambon, et al. 2001. Notch signaling is a direct determinant of keratinocyte growth arrest and entry into differentiation. *EMBO J.* 20:3427–3436.

Rao, P., and T. Kadesch. 2003. The intracellular form of notch blocks transforming growth factor β-mediated growth arrest in Mv1Lu epithelial cells. *Mol. Cell. Biol.* 23:6694–6701.

Raya, A., C.M. Koth, D. Buscher, Y. Kawakami, T. Itoh, R.M. Raya, G. Sternik, H.J. Tsai, C. Rodriguez-Esteban, and J.C. Izpisua-Belmonte. 2003. Activation of Notch signaling pathway precedes heart regeneration in zebrafish. *Proc. Natl. Acad. Sci. USA.* 100:11889–11895.

Seoane, J., C. Pouponnot, P. Staller, M. Schader, M. Eilers, and J. Massagué. 2001. TGFβ influences Myc, Miz-1 and Smad to control the CDK inhibitor p15^{INK4b}. *Nat. Cell Biol.* 3:400–408.

Seoane, J., H.V. Le, L. Shen, S.A. Anderson, and J. Massagué. 2004. Integration of Smad and forkhead pathways in the control of neuroepithelial and glioblastoma cell proliferation. *Cell.* 117:211–223.

Timmerman, L.A., J. Grego-Bessa, A. Raya, E. Bertran, J.M. Perez-Pomares, J. Díez, S. Aranda, S. Palomo, F. McCormick, J.C. Izpisúa-Belmonte, and J.L. De La Pompa. 2004. Notch promotes epithelial-mesenchymal transition during cardiac development and oncogenic transformation. *Genes Dev.* 18:99–115.

Valcourt, U., M. Kowanetz, H. Niimi, C.-H. Heldin, and A. Moustakas. 2005. TGF-β and the Smad signaling pathway support transcriptomic reprogramming during epithelial-mesenchymal cell transition. *Mol. Biol. Cell.* 16:1987–2002.

Zavadil, J., M. Bitzer, D. Liang, Y.C. Yang, A. Massimi, S. Kneitz, E. Piek, and E.P. Böttinger. 2001. Genetic programs of epithelial cell plasticity directed by transforming growth factor-β. *Proc. Natl. Acad. Sci. USA.* 98:6686–6691.

Zavadil, J., L. Cermak, N. Soto-Nieves, and E.P. Böttinger. 2004. Integration of TGF-β/Smad and Jagged1/Notch signalling in epithelial-to-mesenchymal transition. *EMBO J.* 23:1155–1165.